Inverse kinematic tension analysis and optimal design of a cable-driven parallel-series hybrid joint towards wheelchair-mounted robotic manipulator

Shan Zhang[1,2], Dongxing Cao[1,*], Shuai Li[2], Hong Min[2], Feng Fan[3]

1. School of Mechanical Engineering, Hebei University of Technology, Tianjin 300130, China

2. School of Mechatronic Engineering, Zaozhuang University, Zaozhuang 277100, China

3. Xuecheng Human Resources and social Security Bureau, Zaozhuang 277000, China

cad408@sina.com

ABSTRACT. *This paper aims to overcome the inapplicability of the traditional wheelchair-mounted robotic manipulators (WMRMs) to disabled elderly people. To this end, the author proposed a cable-driven parallel-series hybrid joint (CDPSHJ) for the WMRM. The joint is driven by 2 cables between the upper and lower platforms; the two platforms are supported by a middle compression spring, forming the parallel part; the middle of the spring has two rigid shafts with a revolute pair; rigid shaft 1 passes through the upper platform, forming the series part. Then, the inverse kinematic analysis was performed to evaluate the cable length, and the cable tension was analysed through static modelling and lateral buckling modelling of the spring. Then, the correctness of the proposed model was verified by numerical implementations, and the proposed CDPSHJ was proved rational through Matlab simulation. Finally, optimize design based on the inverse kinematics tension analysis. With large work space, smooth motion and light structure, the proposed CDPSHJ is an ideal tool for assistive BCIs.*

RÉSUMÉ. *Cet article a pour objectif de surmonter l'inapplicabilité des manipulateurs robotiques traditionnels montés en fauteuil roulant (WMRMs, le sigle de «Wheelchair-mounted Robotic Manipulator » en anglais) aux personnes âgées handicapées. À cet effet, l'auteur a proposé un joint hybride en série parallèle entraîné par câble (CDPSHJ, le sigle de « cable-driven parallel-series hybrid joint » en anglais) pour le WMRM. Le joint est entraîné par 2 câbles entre les plates-formes supérieure et inférieure; les deux plates-formes sont supportées par un ressort de compression médian, formant la partie parallèle; le milieu du ressort a deux arbres rigides avec une paire révolutionnaire; l'arbre rigide 1 traverse la plate-forme supérieure et forme la pièce en série. Ensuite, l'analyse cinématique inverse a été réalisée pour évaluer la longueur du câble, et la tension du câble a été analysée en fonction de la modélisation statique et modélisation par flambage latéral du ressort. Ensuite, l'exactitude du*

modèle proposé a été vérifiée par des implémentations numériques et le CDPSHJ proposé a été prouvé rationnel par une simulation Matlab. Enfin, l'optimisation de la conception basée sur l'analyse cinématique inverse de la tension est proposée. Avec un grand espace de travail, un mouvement fluide et une structure légère, le CDPSHJ proposé est un outil idéal pour les BCIs fonctionnels.

KEYWORDS: *wheelchair-mounted robotic manipulator (WMRM), cable-driven, hybrid mechanism, spring lateral buckling.*

MOTS-CLÉS: *manipulateur robotique monté en fauteuil roulant (WMRM), câble, mécanisme hybride, flambage latéral du ressort.*

DOI:10.3166/JESA.51.59-74 © 2018 Lavoisier

1. Introduction

The statistics of the World Health Organization (WHO) show that the number of people over the age of 60 will increase from 605 million in 2000 to 2 billion in 2050; In developing countries, the number of old people with no self-care ability is expected to quadruple by 2050 (World Health Organization, 2014). According to *China Statistical Yearbook on the Work for Persons with Disabilities 2013*, China has a total of 37.95 million people of disabilities, among whom 15.64 million (59%) are limb disabled, and the total number is growing at an average annual rate of 6.30% (Sun, 2013). The leading cause of disability among the elderlies is neurodegenerative diseases like stroke, Parkinson's disease, Alzheimer's disease, and amyotrophic lateral sclerosis. Relevant symptoms include paralysis, muscle weakness, gait disorder and excessive pain. Once disabled, the elderly people will have immense difficulty in their activities of daily living (ADLs), namely, reaching, gripping and picking up objects from a shelf or the floor. The long-term care (e.g. assisted living) of these people has become a major social issue. A possible way to solve the problem lies in robotic technology (Hersh, 2015). Of course, this technology has not been fully implemented in real life. For instance, the global sales volume of assistive robots for disabled elderly people was merely 6423 in 2017. Against this backdrop, it is very meaningful to develop an advanced assistive robot to help disabled elderly people with their ADLs. A typical type of the said assistive robot is wheelchair-mounted robotic manipulator (WMRM). It blesses the disabled elderly people with greater independence and better quality of life. The research and development (R&D) of WMRMs can be traced back to the1960s. Over the past 50 years, nearly a dozen WMRMs products have been developed namely, Weston (Hersh, 2015), KARESI-II (Grigorescu *et al.*, 2012), UCF-MANUSI-II, Human-in-the-loop, PerMMA (Jiang *et al.*, 2016), FRIEND system, ASIBOT, Purdue-JACOI-II, Lightweight Robot III (Vogel *et al.*, 2015). However, the products are not widely available in the market, owing to poor usability and low payload.

Table 1 lists some representative commercial WMRMs: Raptor, Manus, JACO, LWA 4D, however, some common problems are found.

Table 1. Four representative commercial WMRMs

Device	Institutions	DOF	Characteristics
Raptor	Applied Resources, US	4	a planar gripper; control with a joystick or a 10-button controller; It cannot be controlled in Cartesian coordinates; lower cost.
Manus	Exact Dynamics, Netherlands	6	two-finger gripper; control with 4×4 button keypad or a joystick; It ensures the gripper remains closed in the event of a power failure; a maximum gripping load of 2 kilograms; It can be folded, reach up to 80 cm and weighs 13 kg.
JACO	Kinova Robotics, Canada	6	a three or a two fingers gripper; It uses carbon fiber to a light-weight (6 kg); a maximum payload of 1.5 kg; It can reach up to 90 cm; control with a three axis joystick; Cartesian controller
LWA4D	SCHUNK, Germany	7	a two fingers SCHUNK gripping system; a maximum payload of 10 kg; Weight of 17.5kg, weight/load capacity ratio of 2:1; Repeat accuracy of ±0.15mm; Position feedback is pseudo-absolute position measurement; Interface of CANopen(CiA DS402:IEC61800-7-201)

First, the manipulator is too heavy. The movement of the WMRMs are rather clumsy due to the mechanical transmission of the manipulator and hand grasping mechanism. To fit in with the large active space, there is no solution but to increase the length and weight of the manipulator. Second, the joints are too bulky. The size of the joints is bloated with the installation of large power-driven motors, decelerators, and various sensors (e.g. encoders and torque sensors). Third, the flexible motion is too limited. Whereas a human hand can grasp an object in a small activity space, a joint of the WMRM has a limited number of DoFs and needs to go through certain sequence transformation before grabbing.

These problems can be ameliorated by the cable-driven mechanism, in which the motor is fixed onto the base. Since its birth in the US and Japan in late 1980s (Tobias Bruckmann & Pott, 2013), the cable-driven mechanism has been applied in various fields, thanks to its low inertia, large workspace, high payload-to-weight ratio, good transportability, ideal reconfigurability and fully remote actuation. The scope of application ranges from large-scale FAST system for a large radio telescope receiver (Zi *et al.*, 2008), to high-speed assembly and pick-and-place operations. Much research has been done on the mechanism. For example, Yang *et al.* (2011) developed a 7DoF anthropopathic cable-driven robotic manipulator. Chen *et al.* (2010) proposed a very similar anthropopathic cable-driven robotic manipulator. Cihat & Pinar, (2017) and Gao *et al.* (2014) probed deep into the humanoid neck mechanism. Similar research results with spring as the support include a flexible elephant trunk robot, a humanoid neck mechanism, a vertebra-based humanoid torso.

Overall, there are few in-depth reports on the bending and compressive of the coil spring which is a common mechanical element in robots. Based on Castigliano's theorem, Reference (Cihat & Pinar, 2017) analyses the variable stiffness characteristics of the compression and bending spring. References (Gao *et al.*, 2014; Yang *et al.*, 2006) treat the spring as a flexible rod for modelling and analysis. Reference (Nori *et al.*, 2007) assumes that the length of the spring and the deformation curvature are both constants. Reference (Cafolla & Ceccarelli, 2016) performs a dynamic simulation of vertebra-based humanoid torso on ADAMS software, and does not conduct any theoretical modelling analysis.

This paper focuses on analyzing the performance of a cable-driven parallel-series hybrid elbow joint (CDPSHEJ) towards WMRA inspired by the three types of humanoid joints. CDPSHEJ is a cable-driven, compression spring supported hybrid mechanism. To the best knowledge of the authors, there are only a few studies to analyze the lateral bending and compression of spring. In this paper the spring lateral bending and compression model is introduced. This model is based on the elliptic integral solution. This method provides better accuracy compared with other for solving the large deflection problems in compliant mechanisms (Zhang & Chen, 2013). Then, the simulation results were analysed in great details to prove the proposed CDPSHEJ rational. In order to decrease the size of actuators, optimal CDPSHEJ structure is performed based on the inverse kinematics analysis and tension analysis.

This paper is organized as follows. The "Design of CDPSHEJ" section presents the concept of CDPSHEJ. Then, the kinematic modelling is presented in "Inverse Kinematics Analysis" section. Next, the "Tension Analysis" section is reported through static modelling and lateral compression and bending modelling of the spring. Then, the MATLAB simulation results are at "Results Analysis" section. Afterwards, optimal joint structure is investigated in "Optimal CDPSHEJ" section. Finally, conclusions stemming from the results are presented in the last section.

2. Design of cdpshej

2.1. Musculoskeletal mechanism of elbow

The compound movement in human upper limb is driven by multiple skeletal muscles around the shoulder, elbow, wrist and hand joints. Previous anatomic studies have shown that the elbow joint is a hinge joint, i.e. the elbow can complete flexion and extension movements. Hence, the elbow joint was identified as a 1DoF joint. As shown in Figure 1, the elbow joint flexes at the contraction of musculus biceps brachii and the relaxation of musculus triceps brachii; the joint extends at the relaxation of musculus biceps brachii and the contraction of musculus triceps brachii.

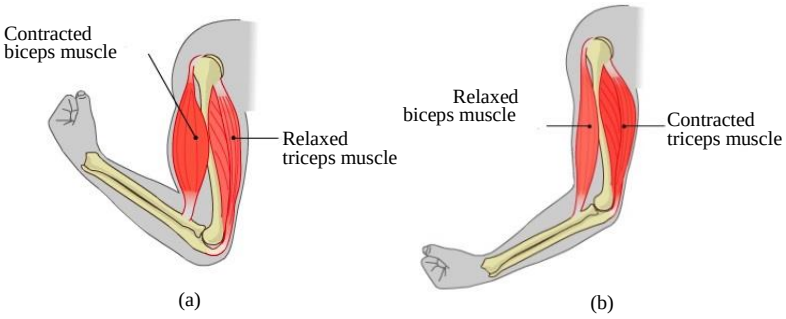

Figure 1. Elbow joint motion mechanism (Physical Education: Structure and function). (a) Elbow flexion. (b) Elbow extension

2.2. Cable-driven elbow joint

Based on the musculoskeletal mechanism of the human elbow joint, an elbow joint driven by 2 cables was designed for WMAMs, considering the advantages of parallel-series hybrid mechanism (e.g. flexible, rigid, accurate, spacious and load-resistant). As shown in Figure 2(a), cable 1, a mimic of musculus biceps brachii, drives the upper platform (moving platform), while cable 2, a mimic of musculus triceps brachii, drives the upper platform; the two platforms are supported by a middle compression spring, forming the parallel part; the middle of the spring has two rigid shafts with a revolute pair; rigid shaft 1 passes through the upper platform, forming the series part. Overall, the CDPSHEJ has a total of 2DoFs.

3. Inverse kinematics analysis

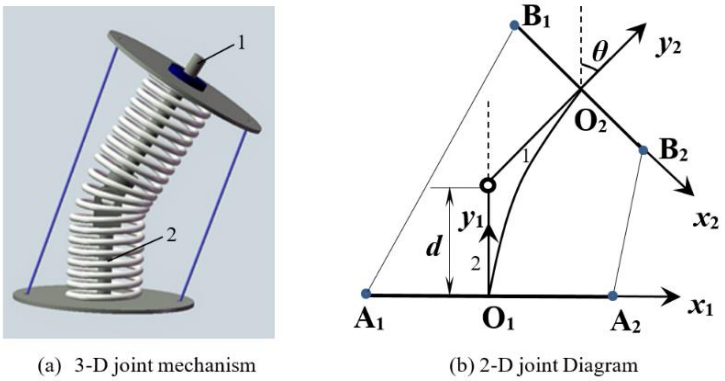

(a) 3-D joint mechanism (b) 2-D joint Diagram

Figure 2. Diagram of the CDPSHEJ

The diagram of the CDPSHEJ is illustrated in Figure 2(b). The upper and lower platforms are designed as thin round plates with a radius of *b* and *a*, respectively. Then, two Cartesian coordinate systems $O_1x_1y_1$ and $O_2x_2y_2$ are fixed to the lower and upper platforms, respectively, with $O_1x_1y_1$ being the global coordinate system. The connecting point of cables 1 and 2 are denoted as A_1, B_1, A_2 and B_2, respectively; the distance from O_1 to the revolute pair centre is denoted as *d.* The spring is simplified as an arc.

As mentioned before, the CDPSHEJ has a total of 2DoFs. One DoF refers to the rotation around the axis Z, and the other the translational motion on the X-Y plane. Under the rigid restraint effect of the middle rotation pair, the relationship of the translational motion relative to O_2 along the X axis and that along the Y axis in the global coordinate system can be expressed as:

$$x = (y - d)tan\theta \tag{1}$$

Therefore, the generalized independent variable of the CDPSHEJ can be defined as (y, θ) and the joint variable as (l_1, l_2), with θ being the rotation angle of the upper platform around the Z axis, and l_1 and l_2 being the lengths of cables 1 and 2, respectively.

It is obvious that the (l_1, l_2) is the output and the translation and rotation of the upper platform (y, θ) is the input of the inverse kinematics analysis. The kinematic relationship between the input and output can be obtained by the closed vector method:

$$\overrightarrow{l_m} = \overrightarrow{A_mB_m} = \overrightarrow{O_1O_2} + \overrightarrow{O_2B_m} - \overrightarrow{O_1A_m} = \overrightarrow{O_1O_2} + {}^{0_1}_{0_2}R\overrightarrow{O_2B_m}^{O_2} - \overrightarrow{O_1A_m} \tag{2}$$

where ${}^{0_1}_{0_2}R = \begin{bmatrix} cos\theta & sin\theta \\ -sin\theta & cos\theta \end{bmatrix}$.

Since m=1,2, the above formula can be expanded as:

$$\overrightarrow{l_1} = \begin{bmatrix} x \\ y \end{bmatrix} + \begin{bmatrix} cos\theta & sin\theta \\ -sin\theta & cos\theta \end{bmatrix}\begin{bmatrix} -b \\ 0 \end{bmatrix} - \begin{bmatrix} -a \\ 0 \end{bmatrix} = \begin{bmatrix} x - bcos\theta + a \\ y + bsin\theta \end{bmatrix};$$

$$\overrightarrow{l_2} = \begin{bmatrix} x \\ y \end{bmatrix} + \begin{bmatrix} cos\theta & sin\theta \\ -sin\theta & cos\theta \end{bmatrix}\begin{bmatrix} b \\ 0 \end{bmatrix} - \begin{bmatrix} a \\ 0 \end{bmatrix} = \begin{bmatrix} x + bcos\theta - a \\ y - bsin\theta \end{bmatrix}.$$

Hence, the lengths of the cables are $l_1 = \|\overrightarrow{l_1}\|$,$l_2 = \|\overrightarrow{l_2}\|$.

4. Tension analysis

The driving cables only work in the tensioning state. Thus, each cable is applied with a tension force. Figure 3 shows the static analysis model of point O_2 point on the upper platform.

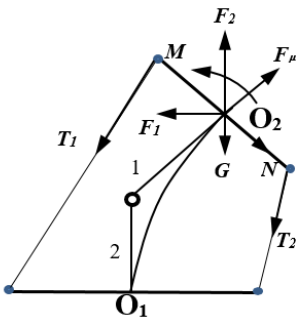

Figure 3. Static analysis model of point O_2

Note: G is the gravity of the upper platform; N is the positive pressure of rigid shaft 1 at point O_2; F_μ is the friction of rigid shaft 1 at point O_2; F_1, F_2 and M are the force/moment with the compression spring acting on point O_2; T_1 and T_2 are tension forces on cables 1 and 2, respectively.

The effects of gravity, positive pressure and friction are negligible due to the small mass of the upper platform. Thus, the static equilibrium equations can be expressed as:

$$\sum_{m=1}^{2} T_m(-\widehat{l_m}) = -\overrightarrow{F_{ext}} \tag{3}$$

$$\sum_{m=1}^{2} {}^{o_1}_{o_2}R\,\overrightarrow{O_2B_m}^{O_2} \times T_m\left(-\widehat{l_m}\right) = -\overrightarrow{M_{ext}} \tag{4}$$

The two formulas can be expanded and merged into:

$$\boldsymbol{ST} = -\boldsymbol{W} \tag{5}$$

Where

$$\widehat{l_m} = \frac{\overrightarrow{l_m}}{l_m},\ \widehat{l_m} = \begin{bmatrix} \widehat{l_{mx}} \\ \widehat{l_{my}} \end{bmatrix},\ \boldsymbol{S_{3\times 2}} = -\begin{bmatrix} \widehat{l_{1x}} & \widehat{l_{2x}} \\ \widehat{l_{1y}} & \widehat{l_{2y}} \\ {}^{o_1}_{o_2}R\overrightarrow{O_2B_1}^{O_2} \times \widehat{l_1} & {}^{o_1}_{o_2}R\overrightarrow{O_2B_2}^{O_2} \times \widehat{l_2} \end{bmatrix}$$

$$\boldsymbol{T_{2\times 1}} = \begin{bmatrix} T_1 \\ T_2 \end{bmatrix}\ \boldsymbol{W_{3\times 1}} = \begin{bmatrix} -F_1 \\ F_2 \\ -M \end{bmatrix}$$

4.1. Modelling of lateral spring compression and bending

Concerning the elastic stability under lateral buckling, the coil compression spring can be treated as an elastic bar, but it must be taken into account the change in the length of the spring due to buckling since the change is not negligible as in the case of compressed bars. Following this train of thought, the compression and bending spring of the CDPSHEJ is subjected to the force analysis as shown in Figure 4.

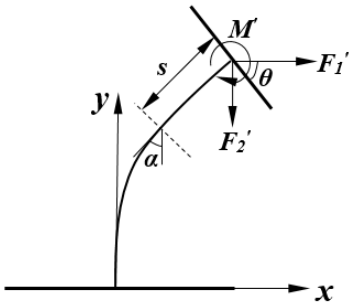

Figure 4. Force analysis diagram of the compression spring

Note: The end forces of the spring satisfy $F_1' = -F_1, F_2' = -F_2$ and $M' = -M$.

Based on the previous static analysis, three equilibrium equations were derived with T_1, T_2, F_1, F_2 and M being unknown quantities. To determine these unknown quantities, the author performed the following modelling analysis of the compression spring.

It is generally agreed in mechanics that the bending moment of an elastic bar equals the product between the bending stiffness and the curvature of bending moment of the bar; the curvature of the elastic bar with large deformation is $\frac{d\alpha}{ds}$, that is:

$$\beta \frac{d\alpha}{ds} = -F_1'y - F_2'x - M' = F_2x + F_1y + M \tag{6}$$

where β is the bending stiffness of the spring.

Find the differential of s in formula (6):

$$\beta \frac{d^2\alpha}{ds^2} = F_1 \frac{dy}{ds} + F_2 \frac{dx}{ds} \tag{7}$$

where $\frac{dy}{ds} = cos\alpha$ and $\frac{dx}{ds} = sin\alpha$.

Multiply both sides of formula (7) with $d\alpha$ and find the integral:

$$\int \beta \frac{d^2\alpha}{ds^2} \cdot \frac{d\alpha}{ds} ds = \int (F_1 cos\alpha + F_2 sin\alpha) d\alpha \tag{8}$$

Let $cos\varphi = F_2/\sqrt{F_1^2 + F_2^2}, sin\varphi = F_1/\sqrt{F_1^2 + F_2^2}$. Formula (8) can be simplified as:

$$\left(\frac{d\alpha}{ds}\right)^2 = -\frac{2}{\beta}\sqrt{F_1^2 + F_2^2} cos(\alpha + \varphi) + C \tag{9}$$

where C is the integral constant determined by the top condition of the bar. Since the bending moment is 0 at top the bar, $C = \frac{2}{\beta}\sqrt{F_1^2 + F_2^2} cos(\theta + \varphi)$ if α=θ and $\frac{d\alpha}{ds} = 0$.

Meanwhile, we have:

$$M = -F_2 x - F_1 y \tag{10}$$

As shown in Figure 4, $\frac{d\alpha}{ds}$ is negative:

$$\frac{d\alpha}{ds} = -\sqrt{\frac{2}{\beta}\sqrt{F_1^2 + F_2^2}(cos(\theta + \varphi) - cos(\alpha + \varphi))} \tag{11}$$

Let x_a be the deflection of an elastic buckling bar in the horizontal direction. Since $\frac{dx}{ds} = sin\alpha$, we have $dx = sin\alpha ds$. Thus $x_a = \int sin\alpha ds$. When α=θ, the horizontal deflection at the top of the bar (O_2):

$$x = \int_0^\theta \frac{sin\alpha d\alpha}{d\alpha/ds} \tag{12}$$

Let $\frac{2}{\beta}\sqrt{F_1^2 + F_2^2} = \mathrm{k}^2$, $\theta + \varphi = \phi$ and $\alpha + \varphi = \gamma$. Thus, $\alpha = \gamma - \varphi$. According to formula (12), we have:

$$x = \int_0^\phi \frac{1}{k}\frac{sin(\gamma - \varphi)}{\sqrt{cos\gamma - cos\phi}} d\gamma \tag{13}$$

Let $p = sin\frac{\phi}{2}$, and introduce the new variable ε. Hence, $sin\frac{\gamma}{2} = psin\varepsilon = sin\frac{\phi}{2}sin\varepsilon$. If α falls between 0 and θ, $sin\varepsilon$ ranges from 0 to 1. Thus, $\varepsilon \in \left[0, \frac{\pi}{2}\right]$. Substituting p and ε into formula (13), we have:

$$xk = x_{\_1} + x_{\_2} \tag{14}$$

where,

$$x_{\_1} = cos\varphi \int_0^{\frac{\pi}{2}} 2\sqrt{2}\, psin\varepsilon d\varepsilon = 2\sqrt{2}pcos\varphi;$$

$$x_{\_2} = -sin\varphi \int_0^{\frac{\pi}{2}} \frac{\sqrt{2} - 2\sqrt{2}p^2 sin^2\varepsilon}{\sqrt{1 - p^2 sin^2\varepsilon}} d\varepsilon.$$

$x_{\_2}$ is the combination of complete elliptic integral of the first kind and completely elliptic integral of the second kind. Obvious, the variable has no analytical solution and only applies to numerical solution.

At this point, the three equilibrium equations obtained from the static analysis were substituted into formulas (10) and (14) to derive the values of T_1, T_2, F_1, F_2 and M.

4.2. Spring parameters

The spring is made of carbon steel. Its parameters are listed in Table 2 below.

Table 2. Spring parameters

E (Gpa)	G (Gpa)	d (mm)	D (mm)	l0 (mm)	n0	K (N/m)
196	78.5	5	40	105	8	23840

Note: E is the elastic modulus; G is the Young's modulus; d is the diameter of spring wire; D is the outer diameter of the spring; l0 is the initial length of the compression spring; n0 is the active coils number of the compression spring. K is the spring constant.

The spring bending stiffness β satisfies the following relationship (Timoshenko & Gere, 1961):

$$\beta = \beta_0 \frac{l}{l_0} \tag{15}$$

where l_0 is the initial length of the spring; l is the compressed length of the spring. Since the spring was treated as an elastic bar of variable length and large deformation, it is assumed that $l = \sqrt{x^2 + y^2} = \|\overrightarrow{O_1O_2}\|$.

Let I be the inertia moment of the cross-section of the spring, and β_0 be the initial bending stiffness of the spring. Then, the two parameters can be expressed as:

$$I = \frac{\pi d^4}{64} = 3.068 \times 10^{-11} \text{ and } \beta_0 = \frac{4EGIl_0}{\pi d n_0 (E + 2G)} = 0.559$$

5. Results analysis

5.1. Inverse kinematics analysis

In the inverse kinematics analysis, the (l_1, l_2) is the output and the translation and rotation of the upper platform (y, θ) is the input. The variable y is introduced to adjust the preload of each cable to (0.085m, 0.095m). The normal ADLs require an elbow extension/flexion of 110° (Raiss *et al.*, 2007). Thus, the value of θ is (-55°, 55°). Because the platform motion is symmetric between (-55°, 0°) and (0°, 55°), the θ value is determined as (0°, 55°).

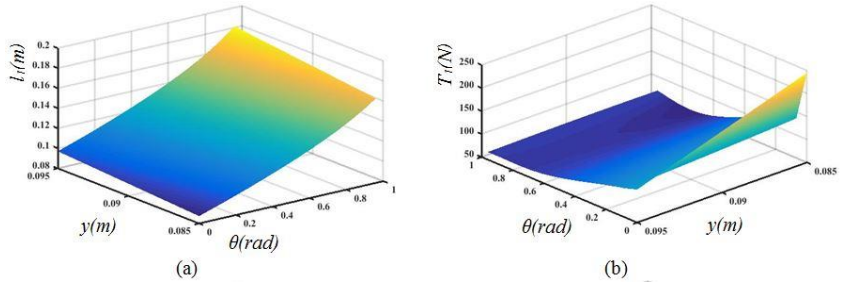

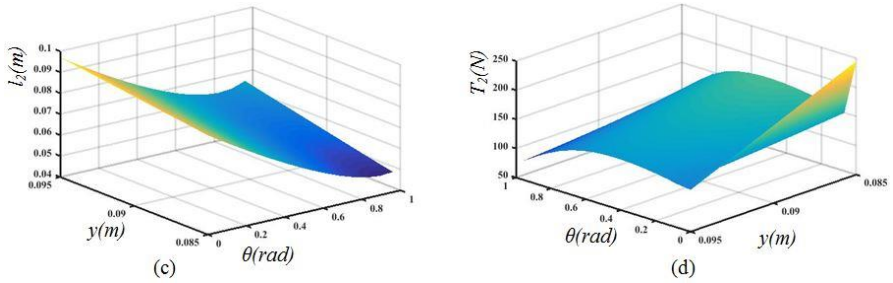

Figure 5. Length and tension of cable 1and 2

The upper and lower platform diameters of cable-driven joint are b=0.05*m* and a=0.07*m*, respectively; the distance between rotation pair and the lower platform is *d*=0.04*m*. These values are inputted into Matlab for simulation. The results are presented in Figure 5.

5.2. Tension analysis

When θ=0°, the spring is linear compression spring. Hence, F_1=0, $F_2 = K(l_0\text{-}y)$, M=0. The cable tension in Figure 5 is analysed through Matlab simulation, aiming to verify the correctness of the spring modelling analysis. Figure 6 shows the results of inverse kinematics analysis and tension analysis at y = 0.085*m*.

As mentioned before, the musculoskeletal mechanism of the elbow joint corresponds to the contraction/relaxation of the musculus biceps brachii and musculus triceps brachii. According to Figures 5 and 6, variation tendency of cables length and tension shows antagonistic characteristics, indicating that the two cables act in a similar way to the muscles of human elbow joint.

The results in Figures 5 and 6 verify the rationality of the CDPSHEJ.

In addition, determine whether ADL are possible, are elbow flexion and extension. As expected, large elbow flexion and extension are needed for most ADLs (Magermans *et al.*, 2005). In other words, the larger the range of motion (RoM) of elbow is, the greater the ability of humanoid arm with shoulder and wrist to perform ADL. With a RoM of 110°, the proposed mechanism satisfies the ADL requirements on elbow extension/flexion. This means the proposed CDPSHEJ is suitable for the WMRM that assists the disabled elderly people in performing ADLs.

As can be seen from Figures 5 and 6, the cable force is positive, indicating that the cables are not slack. When the joint rotated clockwise, the tension of cable 2 is greater than the tension of cable 1. This agrees with the rule of thumb. The above analysis demonstrates the correctness and feasibility of the lateral compression and bending modelling of the spring.

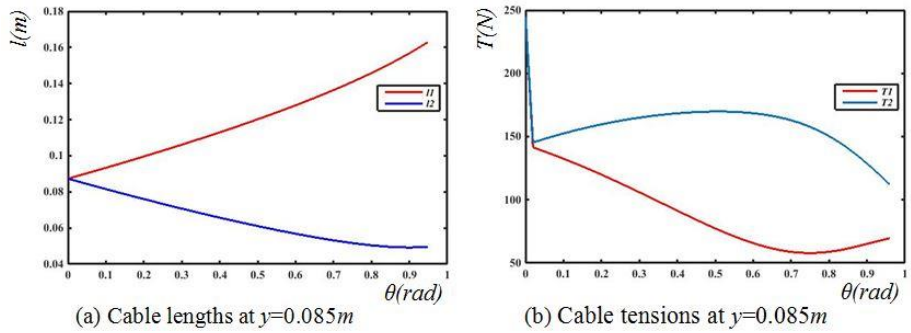

(a) Cable lengths at y=0.085m (b) Cable tensions at y=0.085m

Figure 6. Results of inverse kinematics analysis and tension analysis at y = 0.085m

6. Optimal CDPSHEJ

In order to decrease the size of actuators, optimal CDPSHEJ is performed based on the inverse kinematics analysis and tension analysis. The optimization variables should be *a*, *b*, *d*, which represent the structure variables. The other variables θ, *y* should be specified. Since the optimization objective is to seek smaller motor torque to meet minimal energy consumption, the optimized objective function is T_{max}=max (T_1, T_2), which should be scalar function of *a*, *b*, *d*. Because different *y* can be obtained by pretightening all the two cables simultaneously, and cable tension decreases with the increase of *y* from Figures 5 (b), (d). Therefore, we assume *y* = 0.095 m in the following optimization. When θ=0°, F_1=0, F_2=K(l_0-y), M=0, denote θ as (0°, 55°), which doesn't include 0°. Denote such function as *f(a, b, d)*, then the minimization problem can be generally stated as:

minimize *f(a, b, d)*

subject to $a_l \le a \le a_u$, $b_l \le b \le b_u$, $d_l \le d \le d_u$ and $T_i > 0$ (i = 1, 2)

where a_l, a_u, b_l, b_u, d_l and d_u are bound for *a*, *b* and *d*, respectively, which can be derived from the size of the human upper limb and the spring. Let a_l = b_l = 0.035 m, a_u = b_u = 0.08 m, d_l=0.025m, d_u=0.055m. *f(a, b, d)* is a nonlinear function. As a result, use the nonlinear optimization algorithm in MATLAB Optimization Toolbox to minimize *f*. Choose two different initial points (0.045, 0.035, 0.045) and (0.07, 0.05, 0.04). The optimization final point is all (0.08, 0.0603, 0.025). The final objective function value is all 95.3. Analyse structural parameters *a*, *b*, *d* on optimization objective in order to check the optimization results as the following sections.

6.1. Structural parameters d on objective function

Discretize $a \times b$ into $n \times n$ points, as the same θ, *d*. Traverse $n \times n$ points of (*a*, *b*), to figure out the corresponding objective function values for *d* (*n* points) as shown in Figure 7. Each value in Figure 7 is calculated like this. When *a*, *b* takes a value and

then traverse d (n points) to calculate $f(a, b, d)$ corresponding to the n points of θ from 0° to 55°. If T_1 or T_2 is negative, $f(a, b, d)$ is Inf.

Obviously, when d=0.025m, the objective function value of each curve in Figure 7 is minimum.

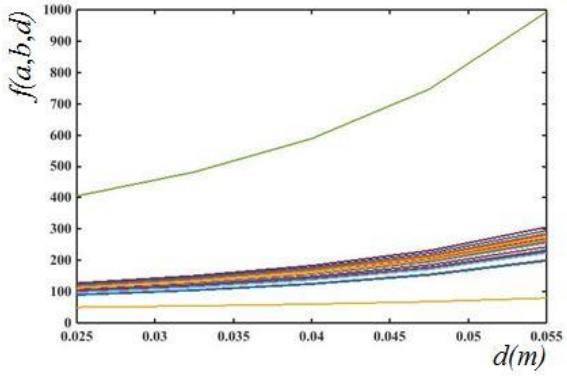

Figure 7. Objective function at traversing a, b

6.2. Structural parameter a, b on objective function

It is known from the previous section that when d=0.025m, $f(a, b, d)$ is minimum. Therefore, let d=0.025m in this part and analyse structural parameters a, b on optimization objective as Figure 8. Traverse a (n points) to figure out the corresponding objective function values for n points of b, as shown in Figure 9. Apparently, when a=0.08m, $f(a, b, d)$ is minimized.

Traverse b (n points) to figure out the corresponding objective function values for n points of a, as shown in Figure 10. Apparently, when b=0.0603m, $f(a, b, d)$ is minimized.

So far, the above analysis results are consistent with the optimization results.

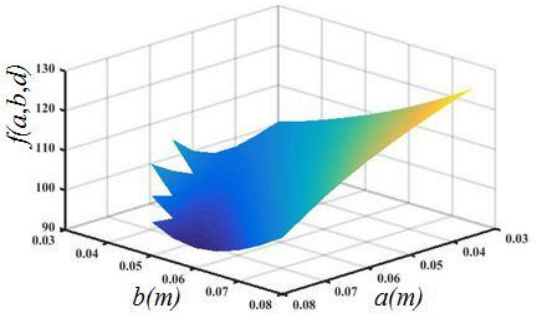

Figure 8. Objective function at d=0.025m

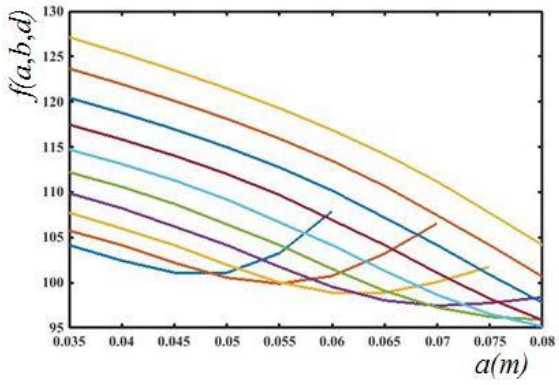

Figure 9. Objective function at traversing b

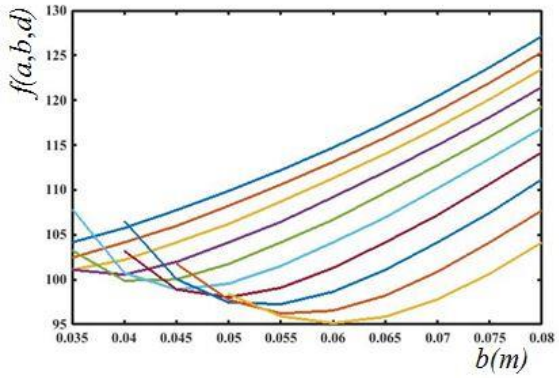

Figure 10. Objective function at traversing a

7. Conclusions

This paper puts forward the CDPSHEJ for WMAMs. After introducing the design, inverse kinematic analysis of the joint is carried out to calculate cable length. Then, the cable tension is analysed through static modelling and lateral compression and bending modelling of the spring. Then, the correctness of the proposed model is verified by numerical implementations, and the proposed CDPSHEJ is proved rational through MATLAB simulation. Finally, based on the inverse kinematics tension analysis optimize design CDPSHEJ. With large workspace, smooth motion and light structure, the proposed CDPSHEJ is an ideal tool for WMRA. The future research will apply variable stiffness properties analysis and closed-loop stiffness control to the joint mechanism, and develop the shoulder and wrist joints (3 or 4 cables-driven) of the anthropopathic manipulator.

Acknowledgments

The work was supported by NSF of China under Grant No. 51275152 and NSF of Hebei Province under Grant No. 2018202114.

References

Cafolla D., Ceccarelli M. (2016). Design and simulation of a cable-driven vertebra-based humanoid torso. *International Journal of Humanoid Robotics*, Vol. 13, No. 4, pp. 1-27. http://doi.org/10.1142/S0219843616500158

Chen Q. Z., Chen W. H., Liu R., Zhang J. B. (2010). Mechanism design and tension analysis of a cable-driven humanoid-arm manipulator with joint angle feedback. *Journal of Mechanical Engineering*, Vol. 46, No. 13, pp. 83-90. http://doi.org/10.3901/JME.2010.13.083

Cihat B. Y., Pinar B. (2017). Design and modeling of a cable-driven parallel-series hybrid variable stiffness joint mechanism for robotics. *Mechanical Sciences*, Vol. 8, No. 1, pp. 65-77. http://doi.org/10.5194/ms-8-65-2017

Dextrous Light weight Arm LWA4D.SCHUNKGmbH&Co.KG. http://www.schunk-modular-robotics.com/en/home/products/dextrous-lightweight-arm-lwa-4d.html

Gao B. T., Song H. G., Zhao J. G., Guo S. X., Sun L. X., Tang Y. (2014). Inverse kinematics and workspace analysis of a cable-driven parallel robot with a spring spine. *Mechanism and Machine Theory*, Vol. 76, pp. 56-69. http://doi.org/10.1016/j.mechmachtheory.2014.01.016

Grigorescu S. M., Lüth T., Fragkopoulos C., Cyriacks M., Gräser A. (2012). A BCI controlled robotic assistant for quadriplegic people in domestic and professional life. *Robotica*, Vol. 30, No. 3, pp. 419-431. http://doi.org/10.1017/S0263574711000737

Hersh M. (2015). Overcoming barriers and increasing independence–service robots for elderly and disabled people. *International Journal of Advanced Robotic Systems*, Vol. 12, No. 114, pp. 1-33. http://doi.org/10.5772/59230

Jiang H. R., Zhang T., Wachs J. P., Duerstock B. S. (2016). Enhanced control of a wheelchair-mounted robotic manipulator using 3-D vision and multimodal interaction. *Computer Vision and Image Understanding*, Vol. 149, pp. 21-31. https://doi.org/10.1016/j.cviu.2016.03.015

Magermans D. J., Chadwick E. K. J., Veeger H. E. J., van der Helm F. C. T. (2005). Requirements for upper extremity motions during activities of daily living. *Clinical Biomechanics*, Vol. 20, No. 6, pp. 591–599. http://doi.org/10.1016/j.clinbiomech.2005.02.006

Nori F., Jamone L., Metta G., Sandini G. (2007). Accurate control of a human-like tendon-driven neck. *Humanoid Robots, 2007 7th IEEE-RAS International Conference on*, pp. 371-378. http://doi.org/10.1109/ICHR.2007.4813896

Physical Education: Structure and function. <http://www.bbc.co.uk/bitesize/standard/pe/the_body/structure_and_function/revision/3/>

Raiss P., Rettig O., Wolf S., Loew1 M., Kasten P. (2007). Range of motion of shoulder and elbow in activities of daily life in 3D motion analysis. *Zeitschrift fur Orthopadie und Unfallchirurgie*, Vol. 145, No. 4, pp. 493-498. http://doi.org/10.1055/s-2007-965468

Sun X. D. (2013). China statistical year book on the work for persons with disabilities. Beijing: China Statistics Press.

Timoshenko S., Gere J. (1961). Theory of elastic stability. New York, NY: McGraw-Hill.

Tobias Bruckmann T., Pott A. (2013). Cable-driven parallel robots. *Mechanisms and Machine Science*, Springer International Publishing. http://doi.org/10.1007/978-3-642-31988-4

Vogel J., Haddadin S., Jarosiewicz B., Simeral J. D., Bacher D., Hochberg L. R., Donoghue J. P., Van Der Smagt P. (2015). An assistive decision-and-control architecture for force-sensitive hand–arm systems driven by human–machine interfaces. *The International Journal of Robotics Research*, Vol. 34, No. 6, pp. 1-18. http://doi.org/10.1177/0278364914561535

World Health Organization (2014). *Facts about ageing*, October 11, 2014. <http://www.who.int/ageing/about/facts/en/>.

Yang G. L., Mustafa S. K., Yeo S. H., Lin W., Lim W. B. (2011). Kinematic design of an anthropomimetic 7-DOF cable-driven robotic arm. *Frontiers of Mechanical Engineering*, Vol. 6, No. 1, pp. 45-60. http://doi.org/10.1007/s11465-011-0205-3

Yang J. Z., Pitarch E. P., Potratz J., Steven Beck S., Abdel-Malek K. (2006). Synthesis and analysis of a flexible elephant trunk robot. *Advanced Robotics*, Vol. 20, No. 6, pp. 631-659. http://doi.org/10.1163/156855306777361631

Zhang A. M., Chen G. M. (2013). A comprehensive elliptic integral solution to the large deflection problems of thin beams in compliant mechanisms. *J Mech Robot*, Vol. 5, No. 2, pp. 021006. http://doi.org/10.1115/1.4023558

Zi B., Duan B. Y., Du J. L., Bao H. (2008). Dynamic modeling and active control of a cable-suspended parallel robot. *Mechatronics*, Vol. 18, No. 1, pp. 1-12. http://doi.org/10.1016/j.mechatronics.2007.09.004